

Ab initio investigation of magnetic ordering in the double perovskite Sr₂NiWO₆

Nafise Rezaei,^{1,*} Tayebhsadat Hashemifar,^{1,2} Mojtaba Alaei,¹
Farhad Shahbazi,¹ S. Javad Hashemifar,¹ and Hadi Akbarzadeh¹

¹*Department of Physics, Isfahan University of Technology, Isfahan 84156-83111, Iran*

²*Department of Physics, Faculty of Science, Shahrekord University, Shahrekord 88186-34141, Iran[†]*

(Dated: April 9, 2019)

Ab initio calculations, GGA/GGA+*U*, are used to propose a spin Hamiltonian for the B-site ordered double perovskite, Sr₂NiWO₆. Our results show that the exchange interaction constants between the next nearest neighbors in both intra- and inter- *ab* plane (J_2 and J_{2c}) are an order of magnitude larger than the ones between the nearest neighbors (J_1 and J_{1c}). Employing the Monte Carlo simulation, we show that the obtained Hamiltonian properly describes the finite temperature properties of Sr₂NiWO₆. Our *ab initio* calculations also reveal a small magnetic anisotropy and non-trivial bi-quadratic interaction between the nearest inter-*ab* plane neighbors, which play essential roles in stabilizing the type-II anti-ferromagnetic ground state of Sr₂NiWO₆.

PACS numbers: 71.70.Gm, 71.15.Mb, 5.10.Ln, 61.12.-q

I. INTRODUCTION

Ordered double perovskites with general chemical formula A₂BB'O₆, have received great attention owing to the magnetic interactions tunable by substitutions on B and B' ions.¹⁻³ For instance the substitution of Mo by W in Sr₂CuMoO₆, tends to decreasing the Curie-Weiss temperature from -116 to -300 K.⁴ The wide variety of A₂BB'O₆ compounds with different A, B, and B' ions represents various novel properties such as colossal magnetoresistance in Sr₂FeMoO₆,⁵ half-metallicity in Sr₂CrWO₆,⁶ multiferroics in Sr₂NiMoO₆,⁷⁻⁹ and Pb₂FeMeO₆ (Me=Nb, Ta, Sb) ceramics^{10,11}, photovoltaics in Bi₂FeCrO₆¹² and Sc₂FeCrO₆¹³ and low dimensional anti-ferromagnetic (AFM) behavior in Ba₂CuB'O₆ and Sr₂CuB'O₆ (B' = W, Te) compounds.¹⁴

In the majority of magnetic ordered double perovskites A₂BB'O₆, B-site, B'-site or both could be occupied by transition metal magnetic ions. For the cases that B is magnetic and B' is a diamagnetic ion, the magnetic ions interact to each other through B-O-B'-O-B bonds (Fig.1). The magnetic B ions can interact to each other through the direct and super-exchange interactions. Due to the large distance between the B ions the direct exchange interaction is negligible, hence the dominant magnetic interaction would be the super-exchange interaction mediated by the B' and O ions. The B-B'-B angle is 90° for the nearest and 180° for the next nearest neighbors (Fig.1), which could make the nearest neighbor (NN) super-exchange interaction much smaller than the next nearest neighbor (NNN) interaction. The dependence of super-exchange interaction on the bond angle is given by the Goodenough-Kanamori-Anderson rules^{15,16}, according which the super-exchange is AFM and its strength is maximum for 180° bond angle.

Typically, ordered double perovskites show low temperature AFM ordering, except for some compounds including La₂BMnO₆ (B = Mg, Co, Ni, Cu) group which represent ferromagnetic (FM) ordering.¹⁷

Sr₂NiWO₆ is an B-site ordered double perovskite in which the magnetic Ni⁺² ion resides on the B site and hexavalent diamagnetic W⁺⁶ ion occupies the B' locations. Its crystalline structure at room temperature is tetragonal and transforms to the cubic symmetry above 520 K. The lattice distortion tilts the Ni-O-W angle from 180° to 165° in the *ab* plane.¹⁸ Sr₂NiWO₆ exhibits a sharp transition to a type-II AFM (AFM-II) spin ordering below the Néel temperature 54 K.^{18,19} Analysis of the spin-wave excitation spectrum indicates that the 90° super-exchange interaction in Sr₂NiWO₆ is much smaller than the 180° one.^{20,21} On the contrary, Iwanaga *et al.* argued that these magnetic interactions in Sr₂NiWO₆ are comparable.¹⁸ Hence, the relative strength of these super-exchange interactions in Sr₂NiWO₆ is a matter of dispute. Furthermore, the existence of a sharp peak in the magnetic susceptibility of Sr₂NiWO₆, unlike Sr₂CuWO₆, is an indication of a three dimensional ordering in this compound.

The frustration of the exchange interactions between the spins could lead to magnetic degeneracy in anti-ferromagnetic materials. The *fcc* magnetic lattice with the anti-ferromagnetic NN and NNN interactions is an example of the frustrated magnets. This lattice is composed of four Heisenberg anti-ferromagnetic cubic sub-lattices, in a way that the sum of first neighboring ion magnetic fields at a given site vanishes. This results to four independent magnetic sub-lattices with AFM ordering. The magnetic moment directions of the sub-lattices are not constrained on each other. Such a freedom to select the relative magnetic moment direction can be lifted by including some higher order exchange interactions such as bi-quadratic interaction or single-ion interaction generated by the spin-orbit effect. Neglecting the small tetragonal distortion in ordered double perovskites like Sr₂NiWO₆, the magnetic lattice turns to be *fcc*, hence

*Electronic address: n-rezaee@ph.iut.ac.ir

[†]The first two authors have equal contributions to this work

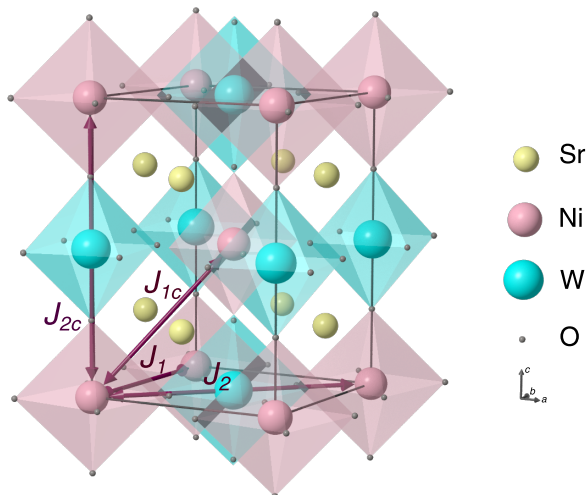


FIG. 1: (Color online) Crystal structure of Sr₂NiWO₆. The thick violet arrows show the nearest and next nearest neighbors at the intra-*ab* plane (J_1 and J_2) and inter-*ab* plane (J_{1c} and J_{2c}), respectively.²²

one expects the emergence of frustration in these compounds. In this work, we study Sr₂NiWO₆ as a prototype of a (rock-salt) ordered double perovskite to shed light on the magnetic features of these compounds. Moreover, the experimental spin-wave excitation spectrum obtained for Sr₂NiWO₆^{20,21} will help us to compare the parameters of our spin Hamiltonian with those extracted by fitting the spin-wave spectrum using linear spin wave theory.

In this study, we employ density functional calculations including Hubbard correction to build a spin model Hamiltonian for Sr₂NiWO₆. We show that the NNN exchange couplings between the intra- and inter- *ab* plane Ni ions are in the same order, which guarantees the three-dimensional magnetic ordering in Sr₂NiWO₆. We also discuss the thermodynamic properties of the obtained model Hamiltonian using classical Monte Carlo (MC) simulation. In addition to the Heisenberg exchange couplings, we consider the bi-quadratic magnetic interaction and magnetic anisotropy interaction in the spin Hamiltonian and argue the key role of these interactions in finding the correct magnetic ground state of Sr₂NiWO₆. To our knowledge, there is no *ab initio* paper which considers the bi-quadratic interaction in these materials.

The paper is organized as the following. Section II discusses the *ab initio* methods to construct the spin Hamiltonian and also the details of MC simulation. The results and discussions are given in section III and section IV is devoted to the conclusions.

II. METHOD

The major part of *ab initio* calculations were done by the Quantum ESPRESSO (QE) package,²³ which

is based on density functional theory (DFT). To treat electron-nucleus interaction, the projector-augmented wave (PAW) pseudo-potentials were employed. The exchange-correlation potential was approximated by the Perdew-Burke-Ernzerhof (PBE) functional within the generalized gradient approximation (GGA).²⁴ To improve the on-site Coulomb repulsion of the localized d electrons, we have applied the GGA+*U* method in a simplified approach by Dudarev,²⁵ which only needs an effective Hubbard parameter (U_{eff}). We used $8 \times 8 \times 6$ k-point meshes for Brillouin zone sampling of the primitive unit cell (which contains two formula units). The experimental crystal structure was taken from Ref. [18]. An energy cutoff of 40 Ry (440 Ry) was chosen for the wave function (electron density) expansion in the plane wave basis set. Higher energy cutoffs were chosen for the lattice and site geometry optimization (50 and 550 Ry for wave function and density expansion, respectively). We have estimated the U_{eff} parameter by using the linear response (LR) method.²⁶ For these calculations, a $2 \times 2 \times 2$ supercell, containing 16 Ni atoms, was used. We employed the full-potential linearized augmented plane wave (LAPW) method, using Fleur code²⁷, to verify PAW pseudo-potentials. For LAPW calculation, we set $k_{\text{max}} = 4.5 \text{ a.u.}^{-1}$, and we chose 2.0, 2.0, 2.2 and 1.4 a.u. for muffin-tin radius of Sr, Ni, W and O, respectively.

To find an effective spin Hamiltonian, the collinear spin-polarized DFT results were mapped to the Heisenberg Hamiltonian given by:

$$H = -\frac{1}{2} \sum_{i,j} J_{ij} \hat{\mathbf{n}}_i \cdot \hat{\mathbf{n}}_j \quad (1)$$

where $\hat{\mathbf{n}}_i$ denotes an unit vector in the direction of the magnetic moment at the *i*-th lattice site, and J_{ij} 's are Heisenberg exchange constants describing the strength of magnetic coupling between the magnetic ions residing on the *i*-th and *j*-th sites. To derive the exchange constants, the DFT total energy of various magnetic configurations were calculated. Then by employing the least-square method, the NN and NNN exchange coupling at the intra-*ab* plane (J_1 , and J_2) and inter-*ab* plane (J_{1c} , and J_{2c}) were computed (Fig. 1).

For the Ni ion with $S = 1$, a bi-quadratic interaction $\sum_{i>j} B_{ij} (\hat{\mathbf{n}}_i \cdot \hat{\mathbf{n}}_j)^2$ is also expected.²⁸ To estimate the bi-quadratic couplings B_{ij} , we used LAPW Fleur code²⁷ which is more specialized for non-collinear spin-polarized DFT. Because of the existence of heavy element W in Sr₂NiWO₆, we investigated the effect of the magnetic anisotropy, $\Delta \sum_i (\hat{\mathbf{n}}_i \cdot \hat{\mathbf{z}})^2$, where Δ denotes the strength of anisotropy. These calculations also were done within LAPW method by including the spin-orbit coupling (SOC) and Hubbard correction (GGA+*U*+SOC).

In the end, we have used classical MC simulations to investigate the finite temperature properties of the obtained spin Hamiltonian. The parallel tempering MC method was carried on a lattice size $N = 2 \times 12^3$, and the uniform temperature range including 64 temperatures was selected. We used 1×10^6 MC steps per spin

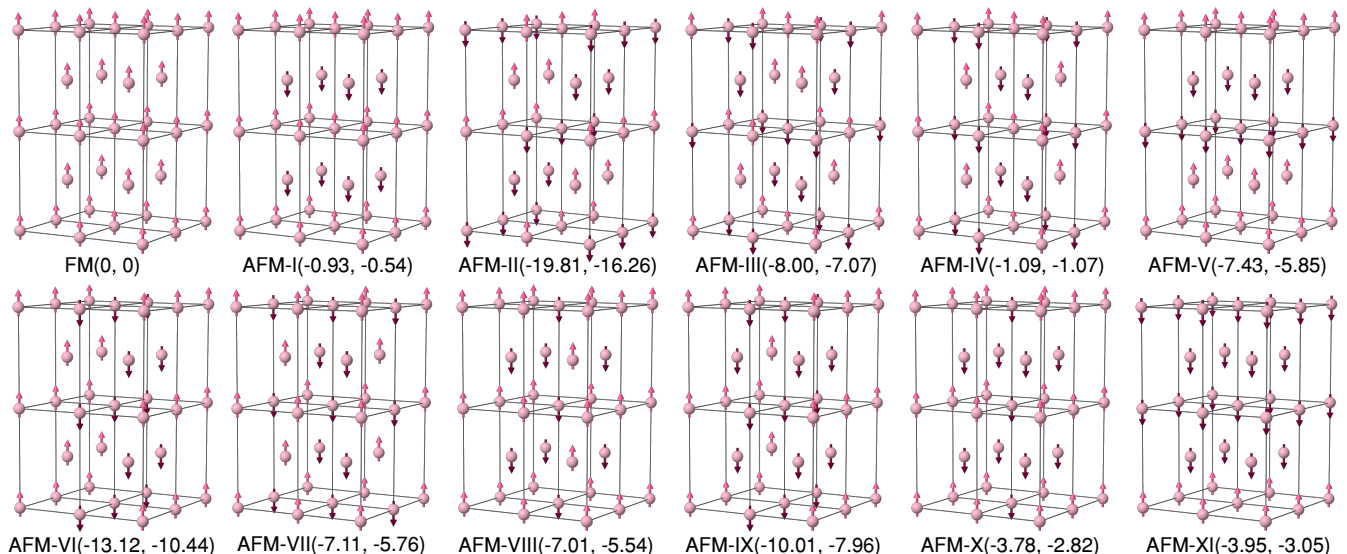


FIG. 2: (Color online) Schematic representation of the Ni spin moments in the various magnetic configurations used for calculating the exchange constants. The numbers in parentheses are the total energy difference of each magnetic configuration (meV/f.u.) respect to the ferromagnetic (FM) configuration for $U_{\text{eff}} = 5$ and 4.72 eV, respectively.

for equilibration and 1×10^6 MC steps for sampling. To reduce the correlation between the data, we skipped 10 MC steps between the data collections. In parallel tempering algorithm, we allowed the spin configurations at the different temperatures to swap with each other after 10 MC steps.

III. RESULTS AND DISCUSSION

A. Spin Hamiltonian

Sr_2NiWO_6 crystallizes in the tetragonal space group $I4/m$ with cell parameters ($a=5.5571$, $c=7.9133$ Å).¹⁸ As shown in Fig. 1, the transition metal ions including the magnetic Ni^{+2} ions and non-magnetic W^{+6} ions are located at the center of the oxygen octahedra. In order to have an insight into the DFT magnetic ground state, different magnetic configurations are considered, as presented in Fig. 2. The calculations are performed within GGA, and GGA+ U approximations for the experimentally-identified as well as *ab initio* optimized crystal structures. For any on-site Hubbard parameter U_{eff} varying from 0 to 7 eV, the magnetic ground state of Sr_2NiWO_6 is the AFM-II ordering (Fig.2), consistent with the experimental observation.^{20,21} In AFM-II, each Ni ion aligns its moment parallel to the half and anti-parallel to the other half of its nearest neighbors, whose number is 4 in *ab* plane and 8 out of this plane. However, for both the intra- and inter- *ab* plane NNN the direction of magnetic moments are anti-parallel (Fig.2).

To evaluate the on-site coulomb repulsion U_{eff} , we use

the linear response (LR) method.²⁶ In LR approach, a perturbed repulsive coulomb interaction is applied as a small shift of potential on d levels such that the response of system to this perturbation remains linear. Using the experimental structure of Sr_2NiWO_6 , the U_{eff} converges to 6.2 eV for Ni, independent of magnetic ordering. Therefore, in the GGA+ U calculations with the experimental structure we take the values 5, 6, and 7 eV for the Hubbard parameter.

To obtain consistent results in an *ab initio* theory, one needs to include all relevant details such as optimized structural geometry. Therefore, using the GGA+ U , we optimize structural geometry. For a fully consistent result, we also estimate U_{eff} in a self-consistent LR (SCLR) scheme²⁹. For this purpose, in each step, the crystal structure are optimized in the GGA+ U calculation with the value of U parameter obtained from the previous step. Given the new structure, the value of U is updated in the SCLR scheme. Iterating this process makes the value of U to converge to a constant. Starting from $U_{\text{eff}} = 6.2$ eV of the experimental structure, we find that the on-site Hubbard parameter converge to 4.72 eV. The total energy difference of the considered magnetic configurations and the FM state are reported in Fig. 2 for the experimental structure and *ab initio* optimized structure with $U_{\text{eff}} = 5$ eV and $U_{\text{eff}} = 4.72$ eV, respectively.

Now, we proceed to find the spin Hamiltonian. For this purpose, we map the resulting total energies onto the Heisenberg Hamiltonian. The relevant exchange constants (J_1, J_{1c}, J_2, J_{2c}), for the experimental structure with $U_{\text{eff}} = 0, 5, 6, 7$ eV and the optimized structure with $U_{\text{eff}} = 4.72$ eV are listed in table I, showing that all the couplings are AFM. The details of this calcula-

TABLE I: Obtained exchange constants (meV) and Néel temperature T_N (K) at different values of the Hubbard parameter (eV) for experimental and optimized crystal structures of Sr_2NiWO_6 within PAW and LAPW method. The calculations (PAW/GGA+ U) with $U_{\text{eff}} = 0, 5, 6, 7$ eV were done in the experimental structure and the one with $U_{\text{eff}} = 4.72$ eV corresponds to the optimized structure. All of LAPW calculations have been done by using experimental structure. The last row indicate INS results for exchange parameters²⁰. For each exchange parameters set (except INS results), T_N is derived from MC simulations.

	U_{eff} (eV)	J_1 (meV)	J_{1c} (meV)	J_2 (meV)	J_{2c} (meV)	T_N (K)
PAW	0	-0.36	-0.34	-8.06	-9.07	139
	5	-0.16	-0.12	-3.06	-3.45	52
	6	-0.14	-0.10	-2.52	-2.83	43
	7	-0.11	-0.08	-2.05	-2.30	35
	4.72	-0.24	-0.05	-2.44	-2.90	43
LAPW	0	-0.54	-0.47	-8.22	-10.18	146
	5 ($U = 6.0, J_H = 1.0$)	-0.27	-0.18	-1.87	-2.90	36
Exp. (INS) ²⁰		-0.02 ± 0.08		-1.81 ± 0.09		$54^{18,19}$

tion are given in Appendix A. The small difference between the energy of AFM-I and FM magnetic configurations (see Fig. 2) justifies the smallness of the inter- ab plane NN coupling J_{1c} . Indeed one can simply find $J_{1c} = (E_{\text{AF-I}} - E_{\text{FM}})/8$.

Table I also shows that NNN coupling constants (J_2, J_{2c}) are an order of magnitude larger than the NN ones (J_1, J_{1c}). Indeed the 90° Ni-W-Ni bond angle in both intra- and inter- ab planes makes the super-exchange interaction between the NN magnetic ions too weak. On the other hand, the Ni-W-Ni angle for both the intra- and inter- ab plane NNN ions is 180° which substantially enhances the NNN exchange constants. Moreover, the Ni-O-W bond angle in the intra- ab plane (165.8°) is slightly smaller than the corresponding bond angle in the inter- ab plane (180°), which somewhat enhances J_{2c} compared with J_2 . It can be seen from table I that the coupling constants decrease by increasing U_{eff} , which is a consequence of attenuating the hopping amplitude of neighboring d electrons as the expense of enlarging the on-site Coulomb repulsion.

To check how the exchange constants depend on the method, we employ the LAPW method and compare its results to those obtained by PAW. For GGA (i.e. $U = 0$) there is 10% (in average) discrepancy in exchange constants between the two methods which is reasonable. We repeat the LAPW calculation using GGA+ U . It is worthy to mention that GGA+ U implementation in Fleur LAWP code is based on Liechtenstein's approach³⁰ which includes two parameters; U as on-site Coulomb repulsion and J_H as on-site (Hund) exchange. However, in the PAW/GGA+ U method we employ the Dudarev's approach²⁵ which uses only one parameter i.e. U_{eff} . Generally, the relationship between U_{eff} , U and J_H is $U_{\text{eff}} = U - J_H$. Knowing that in many oxides $J_H \sim 1$ eV^{31,32}, in this work we set J_H to 1 eV. In principle, one has to calculate U and J_H in LAPW/GGA+ U but as a rough approximation, we use $U = U_{\text{eff}} + J_H$ where U_{eff} is the PAW value. The exchange parameters

obtained by LAPW/GGA+ U ($U = 6.0, J_H = 1.0$ eV) are reported in Table I. These results are comparable with those obtained by PAW when $U_{\text{eff}} = 5 - 6$ eV is used.

Linear spin-wave (LSW) fitting of excitation spectrum obtained by inelastic neutron scattering (INS) experiment, results in $J_1 \approx -0.02$ meV and $J_2 \approx -1.81$ meV.^{20,21} The discrepancy between our result and LSW comes from the linear approximation in LSW which yields an error of the order of $1/S$ (which for $S = 1$ could be large). We will further discuss the INS result in subsection III B.

Now we consider the bi-quadratic interaction between the NN along inter- ab planes. The dependence of the total energy on angle between the Ni magnetic moments reveals that if there is the bi-quadratic interaction in this compound. The Ni^{+2} ions in Sr_2NiWO_6 are located in the lattice points of two tetragonal sub-lattices shifted by $(a/2, a/2, c/2)$. To calculate the bi-quadratic coupling constants B_{ij} , starting from a FM configuration, we compute the total energy of the magnetic configurations in which the direction of the magnetic moments in these two sub-lattices are rotated by the angle θ .

Fig. 3 presents the variation of energy ($\Delta E = E(\theta) - E(\theta = 90^\circ)$) for GGA (i.e. $U_{\text{eff}} = 0$) and GGA+ U ($U_{\text{eff}} = 5$ eV) with the experimental structure. The ΔE - θ curve can be well fitted by the function $f(x) = 8(B \cos^2 \theta - J_{1c} \cos \theta)$ which comes from the spin Hamiltonian containing only the inter- ab plane NN Heisenberg and bi-quadratic interactions (the NNN interactions do not have any contribution in ΔE). As a result, there is a bi-quadratic interaction in Sr_2NiWO_6 in both of GGA and GGA+ U . The bi-quadratic coupling constant is negative and its value is, $B \approx -0.03$ and -0.04 meV for $U_{\text{eff}} = 0$ and 5 eV, respectively. Similar results is obtained if we use the optimized crystal structure with $U_{\text{eff}} = 4.72$ eV.

Finally we investigate the single-ion anisotropy arising from the spin-orbit effect. The single-ion term can

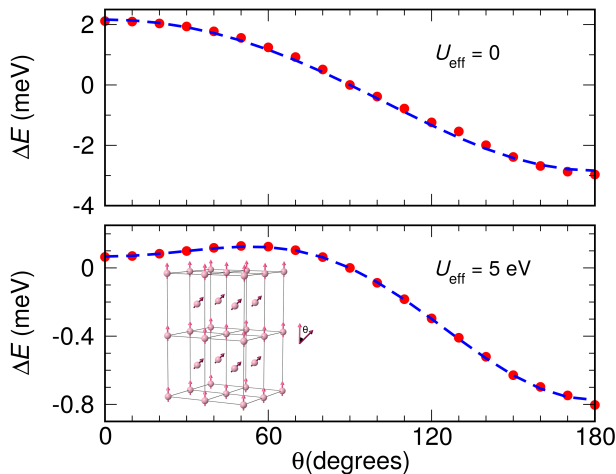


FIG. 3: (Color online) Total energy versus rotational angle θ (the angle between the magnetic moments of the two tetragonal sub-lattices). The reference of energy is set to $\theta = 90^\circ$. The dash line denotes the fit to the data using the function $f(x) = 8(B \cos^2 \theta - J_{1c} \cos \theta)$.

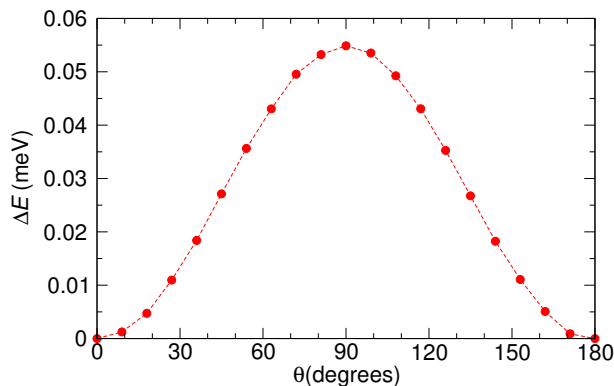


FIG. 4: (Color online) Total energy versus rotational angle θ respect to the lattice c -axis within GGA+ U +SOC. The reference of energy is set to $\theta = 0^\circ$.

be written as $\Delta \sum_i (\hat{\mathbf{n}}_i \cdot \hat{\mathbf{d}})^2$, where $\hat{\mathbf{d}}$ denotes the easy axis direction. We assume that $\hat{\mathbf{d}}$ is along lattice c -axis (see Fig. 1). Using GGA+ U +SOC with $U_{\text{eff}} = 5$, we calculated the total energy for the FM spin configuration as the angle θ (the angle between the magnetic moment direction and z -axis) varies from 0 to π . Fig. 4 shows the variation of ΔE versus θ . This figure represent that the minimum energy is achieved at $\theta = 0$. The value of Δ from this calculation is ≈ -0.05 meV, whose sign indicates that z -axis is indeed an easy axis. We also checked that the total energy is independent of the azimuthal angle ϕ . It should be noted that the two-spin Ising anisotropy ($J_z S_{i,z} S_{j,z}$) may have contribution to the energy difference curve in Fig. 4. Nevertheless, it is hard to separate its contribution since both single-ion

and Ising anisotropy terms have the same angular dependence for uniform rotation of spin direction. Due to this limitation we assign it totally to the single-ion anisotropy.

B. Monte Carlo Simulation

For investigating the finite temperature behavior of the spin Hamiltonian we carry on classical MC simulations, using the coupling constants obtained by $U_{\text{eff}} = 0, 5, 6, 7$ eV in experimental and $U_{\text{eff}} = 4.72$ eV in optimized structure. It is found that all the spin Hamiltonians, containing NN and NNN Heisenberg couplings (given in Table I) and NN inter- ab plane bi-quadratic terms ($B = J_{1c}$), in both experimental and optimized structures and the exchange couplings show a transition to a AFM-II ordering with the Néel temperatures (T_N) given in Table I. Comparing the measured $T_N \approx 54$ K^{18,19}, we find that taking $U_{\text{eff}} \approx 5$ eV would be fine choice for the experimental structure. Moreover, in the optimized structure, the T_N obtained by SCLR value $U_{\text{eff}} = 4.72$ eV in a good agreement with the experimentally measured value. The SCLR method gives reasonable results for the compounds whose bonds have high ionic character. Using Critic2 code^{35,36}, we find the following valence state based on Bader charge analysis: $\text{Sr}_2^{+1.60} \text{Ni}^{+1.39} \text{W}^{+3.00} \text{O}_6^{-1.26}$. The charge analysis shows that the nature of Ni-O bonds in Sr_2NiWO_6 are predominantly ionic, which is the reason that SCLR works for this compound.

The exchange constants obtained by INS, result to $T_N = 34$ K in the MC simulation which is 40% less than experimental value T_N (54 K). This discrepancy, as already discussed, could be due to the using LSW for $S = 1$ which underestimates the value of J_2 .

It should be mentioned that the bi-quadratic and single-ion interactions do not have much effect on T_N , nevertheless we will show in the following that they have an essential role in singling out a collinear spin configuration.

To gain an insight into the low temperature magnetic ordering in MC simulations, we calculate the average spin-spin correlation at $T = 4$ K. Fig. 5 represents the averages of the products of neighboring spins ($\langle S_i \cdot S_j \rangle$) and also their absolute values ($\langle |S_i \cdot S_j| \rangle$) for the spin Hamiltonian given by the couplings obtained by $U_{\text{eff}} = 5$ eV. As can be seen from this figure regardless of absence or presence of the bi-quadratic and single-ion interactions, $\langle S_i \cdot S_j \rangle$ is ≈ 0 for both intra- and inter- ab plane NN spins and ≈ 1 for all NNN spins. However, for the NN spins the value of $\langle |S_i \cdot S_j| \rangle$ is less than 1 (≈ 0.5) in absence of bi-quadratic term or single-ion term and about 1 when including one or both of these interactions ($B \approx -0.04$, $\Delta \approx -0.05$ eV). These calculations show that when both B and Δ are zero, the magnetic moments have freedom to rotate with respect to their nearest neighbors, however when either B or Δ is turned on they loss their freedom and fix their directions parallel or anti-parallel to their

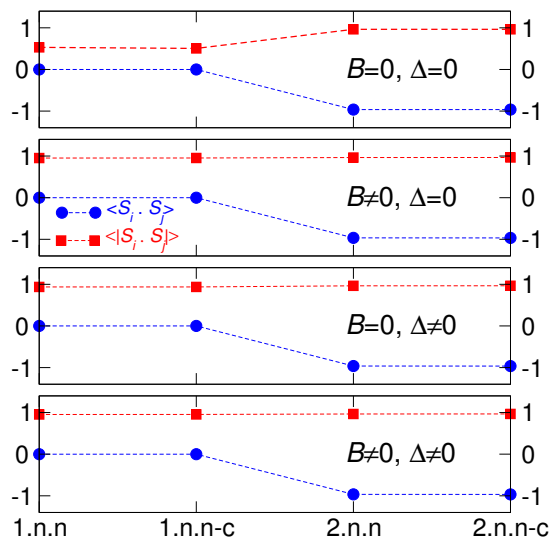


FIG. 5: (Color online) Average (absolute) spin-spin correlation of intra- and inter- ab plane NN and NNN obtained by MC simulations at $T = 4$ K with the derived exchange parameters using $U_{\text{eff}} = 5$ eV.

neighbors, hence stabilizing the collinear configuration AFM-II. Indeed, the freedom of magnetic moments to rotate would give rise to residual entropy at the low temperatures, however the experimental results don't show such an entropy.¹⁹

Our MC simulations show that the ground state of Sr_2NiWO_6 is doubly degenerate. This can be verified by calculating the elastic neutron scattering structure function given by

$$S(\mathbf{q}) = \sum_{i,j} \langle (\mathbf{S}_i - \frac{\mathbf{S}_i \cdot \mathbf{q}}{\mathbf{q} \cdot \mathbf{q}} \mathbf{q}) \cdot (\mathbf{S}_j - \frac{\mathbf{S}_j \cdot \mathbf{q}}{\mathbf{q} \cdot \mathbf{q}} \mathbf{q}) \rangle \exp[i\mathbf{q} \cdot (\mathbf{R}_i - \mathbf{R}_j)] \quad (2)$$

Indeed, different MC runs end in two collinear spin configurations AFM-II and AFM-IIb illustrated in Fig. 6. The difference between these two configurations are the rotation of the $(0, 0, 2)$ planes (highlighted in gray) by 90° with respect to the $(0, 0, 1)$ planes along the c direction. The right panels in Fig. 6 show the density plots of $S(\mathbf{q})$ for these two spin configurations. The main difference between the pattern of $S(\mathbf{q})$ for these two spin configurations is the elimination of some Bragg peaks in AFM-II.

While AFM-II and AFM-IIb are classically degenerate, it has been shown that in large S limit the quantum effects lift the degeneracy of these two magnetic configurations in favor of AFM-II.³⁷

IV. CONCLUSIONS

In summary, we studied the magnetic interactions and thermodynamic properties of Sr_2NiWO_6 , using *ab ini-*

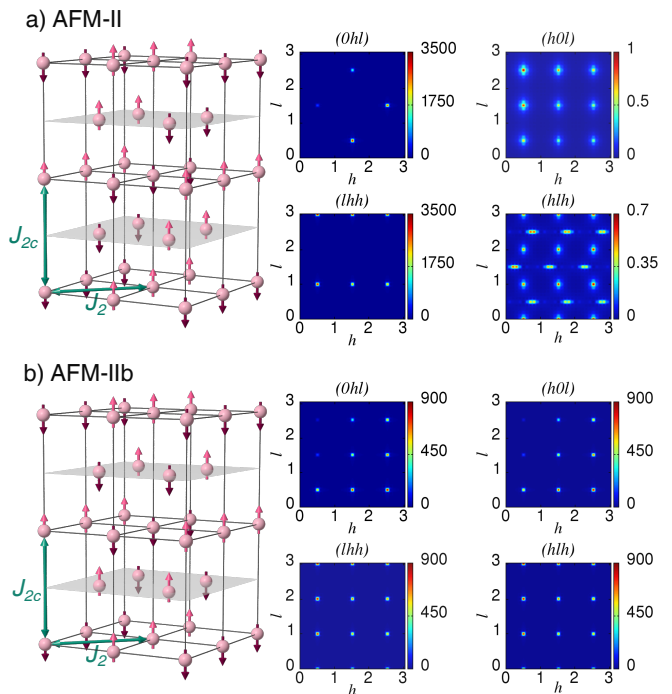


FIG. 6: (Color online) A schematic of the type-II anti-ferromagnetic (AFM-II) and type-IIb anti-ferromagnetic (AFM-IIb) ordering and their MC neutron structure factor, $S(\mathbf{q})$, in the $(0hl)$, $(h0l)$, (lhh) and (hlh) planes at $T = 4$ K by including the Heisenberg, bi-quadratic and anisotropy terms in spin Hamiltonian which derived from GGA+ U ($U_{\text{eff}} = 5$ eV).

tio GGA and GGA+ U calculations and classical Monte Carlo simulation. We found that interactions of the next nearest neighbors in the intra- and inter- ab plane, bi-quadratic interaction between inter- ab plane nearest neighbors and the magnetic anisotropy along the \hat{z} , are the key players in determining the magnetic ordering of this compound. Our results show that the classical ground state of Sr_2NiWO_6 has double degeneracy denoted by AFM-II and AFM-IIb. The elastic neutron scattering structure factors corresponding to these two magnetic configurations were calculated and presented as reliable theoretical references for experimental refinement of the true magnetic ground state of this compound by using neutron scattering experiments.

Acknowledgments

N.R and H.A acknowledge the support of the National Elites Foundation and Iran National Science Foundation:INSF. We acknowledge Hojjat Gholizadeh for his help to use POV-Ray.

- ¹ S. Vasala and M. Karppinen, Progress in Solid State Chemistry **43**, 1 (2015).
- ² C. J. Howard, B. J. Kennedy, and P. M. Woodward, Acta Crystallographica Section B **59**, 463 (2005).
- ³ A. Hossain, P. Bandyopadhyay, and S. Roy, Journal of Alloys and Compounds **740**, 414 (2018), ISSN 0925-8388, URL <http://www.sciencedirect.com/science/article/pii/S092583881734478X>.
- ⁴ S. Vasala, H. Saadaoui, E. Morenzoni, O. Chmaissem, T.-S. Chan, J.-M. Chen, Y.-Y. Hsu, H. Yamauchi, and M. Karppinen, Phys. Rev. B **89**, 134419 (2014).
- ⁵ T. Kimura, H. Sawada, and K. Terakura, Nature **395**, 677 (1998).
- ⁶ J. B. Philipp, P. Majewski, L. Alff, A. Erb, R. Gross, T. Graf, M. S. Brandt, J. Simon, T. Walther, W. Mader, et al., Phys. Rev. B **68**, 144431 (2003).
- ⁷ H. Hsu, P. Blaha, and R. M. Wentzcovitch, Physical Review B **85**, 140404 (2012).
- ⁸ S. Kumar, G. Giovannetti, J. van den Brink, and S. Picozzi, Phys. Rev. B **82**, 134429 (2010).
- ⁹ A. Prasatkhetragarn, s. Kaowphong, and R. Yimnirun, Applied Physics A **107**, 117 (2012).
- ¹⁰ A. A. Gusev, S. I. Raevskaya, V. V. Titov, V. P. Isupov, E. G. Avvakumov, I. P. Raevski, H. Chen, C.-C. Chou, S. P. Kubrin, S. V. Titov, et al., Ferroelectrics **496**, 231 (2016), <https://doi.org/10.1080/00150193.2016.1157742>, URL <https://doi.org/10.1080/00150193.2016.1157742>.
- ¹¹ V. V. Laguta, V. A. Stephanovich, M. Savinov, M. Marysko, R. O. Kuzian, I. V. Kondakova, N. M. Olekhnovich, A. V. Pushkarev, Y. V. Radyush, I. P. Raevski, et al., New Journal of Physics **16**, 113041 (2014), URL <http://stacks.iop.org/1367-2630/16/i=11/a=113041>.
- ¹² R. Nechache, W. Huang, S. Li, and F. Rosei, Nanoscale **8**, 3237 (2016), URL <http://dx.doi.org/10.1039/C5NR08819D>.
- ¹³ T.-Y. Cai, S.-C. Liu, S. Ju, C.-Y. Liu, and G.-Y. Guo, Phys. Rev. Applied **8**, 034034 (2017), URL <https://link.aps.org/doi/10.1103/PhysRevApplied.8.034034>.
- ¹⁴ D. Iwanaga, Y. Inaguma, and M. Itoh, Journal of Solid State Chemistry **147**, 291 (1999).
- ¹⁵ J. B. Goodenough, Phys. Rev. **100**, 564 (1955), URL <https://link.aps.org/doi/10.1103/PhysRev.100.564>.
- ¹⁶ J. Kanamori, Journal of Physics and Chemistry of Solids **10**, 87 (1959), ISSN 0022-3697, URL <http://www.sciencedirect.com/science/article/pii/0022369759900617>.
- ¹⁷ G. Blasse, Journal of physics and Chemistry of Solids **26**, 1969 (1965).
- ¹⁸ D. Iwanaga, Y. Inaguma, and M. Itoh, Materials Research Bulletin **35**, 449 (2000).
- ¹⁹ C. G. F. Blum, A. Holcombe, M. Gellesch, M. I. Sturza, S. Rodan, R. Morrow, A. Maljuk, P. Woodward, P. Morris, A. U. B. Wolter, et al., Journal of Crystal Growth **421**, 39 (2015), ISSN 0022-0248.
- ²⁰ Y. Todate, Journal of Physics and Chemistry of Solids **60**, 1173 (1999).
- ²¹ Y. Todate, Activity Report on Neutron Scattering Research (ISSP) **2**, 127 (1995).
- ²² D. K. Buck and A. A. Collins, lattice pictures rendered with POV-Ray., URL <http://www.povray.org/>.
- ²³ P. Giannozzi, S. Baroni, N. Bonini, M. Calandra, R. Car, C. Cavazzoni, D. Ceresoli, G. L. Chiarotti, M. Cococcioni, I. Dabo, et al., Journal of Physics: Condensed Matter **21**, 395502 (2009).
- ²⁴ J. P. Perdew, K. Burke, and M. Ernzerhof, pp. 3865–3868 (1996).
- ²⁵ S. L. Dudarev, G. A. Botton, S. Y. Savrasov, C. J. Humphreys, and A. P. Sutton, Phys. Rev. B **57**, 1505 (1998).
- ²⁶ M. Cococcioni and S. de Gironcoli, Phys. Rev. B **71**, 035105 (2005).
- ²⁷ FLEURgroup, <http://www.flapw.de/>.
- ²⁸ F. Patrik, *Lecture notes on electron correlation and magnetism*, vol. 5 (World scientific, 1999).
- ²⁹ H. J. Kulik, M. Cococcioni, D. A. Scherlis, and N. Marzari, Phys. Rev. Lett. **97**, 103001 (2006).
- ³⁰ A. I. Liechtenstein, V. I. Anisimov, and J. Zaanen, Phys. Rev. B **52**, R5467 (1995), URL <http://link.aps.org/doi/10.1103/PhysRevB.52.R5467>.
- ³¹ V. I. Anisimov, J. Zaanen, and O. K. Andersen, Phys. Rev. B **44**, 943 (1991), URL <https://link.aps.org/doi/10.1103/PhysRevB.44.943>.
- ³² L. Vaugier, H. Jiang, and S. Biermann, Phys. Rev. B **86**, 165105 (2012), URL <https://link.aps.org/doi/10.1103/PhysRevB.86.165105>.
- ³³ A. Rohatgi, *Webplotdigitizer*, <https://automeris.io/WebPlotDigitizer>.
- ³⁴ T. Datta and D.-X. Yao, Phys. Rev. B **85**, 054409 (2012), URL <https://link.aps.org/doi/10.1103/PhysRevB.85.054409>.
- ³⁵ A. O. de-la Roza, E. R. Johnson, and V. Luaa, Computer Physics Communications **185**, 1007 (2014), ISSN 0010-4655, URL <http://www.sciencedirect.com/science/article/pii/S0010465513003718>.
- ³⁶ A. O. de-la Roza, M. Blanco, A. M. Pends, and V. Luaa, Computer Physics Communications **180**, 157 (2009), ISSN 0010-4655, URL <http://www.sciencedirect.com/science/article/pii/S0010465508002865>.
- ³⁷ T. Yildirim, A. B. Harris, and E. F. Shender, Physical Review B **58**, 3144 (1998).

Appendix

A. Details about total energies of all our configurations

The total energies for eight formula units without considering the nonmagnetic part, by Heisenberg Hamiltonian for ferromagnetic ordering can be written as:

$$E_{FM} = (32J_1 + 64J_{1c} + 32J_2 + 16J_{2c})S^2 \quad (3)$$

and for considered AFM orderings would be as:

$$\begin{aligned}
E_I &= (32J_1 - 64J_{1c} + 32J_2 + 16J_{2c}) S^2 \\
E_{II} &= (0J_1 + 0J_{1c} - 32J_2 - 16J_{2c}) S^2 \\
E_{III} &= (-32J_1 + 0J_{1c} + 32J_2 - 16J_{2c}) S^2 \\
E_{IV} &= (-32J_1 + 0J_{1c} + 32J_2 + 16J_{2c}) S^2 \\
E_V &= (32J_1 + 0J_{1c} + 32J_2 - 16J_{2c}) S^2 \\
E_{VI} &= (0J_1 + 0J_{1c} - 32J_2 + 16J_{2c}) S^2 \\
E_{VII} &= (-16J_1 + 0J_{1c} + 0J_2 + 16J_{2c}) S^2 \\
E_{VIII} &= (0J_1 - 16J_{1c} + 0J_2 + 16J_{2c}) S^2 \\
E_{IX} &= (0J_1 + 0J_{1c} - 16J_2 + 16J_{2c}) S^2 \\
E_X &= (16J_1 - 32J_{1c} + 16J_2 + 16J_{2c}) S^2 \\
E_{XI} &= (32J_1 + 0J_{1c} + 32J_2 + 0J_{2c}) S^2
\end{aligned}$$

In table II we gather and compare the GGA+U/PAW total energy with its counterpart Heisenberg Hamiltonian. The mean absolute error of Heisenberg Hamiltonian energy respect to GGA+U/PAW total energy is about 0.07 meV/f.u. .

TABLE II: The total energy difference of different magnetic configurations (meV/f.u.) with respect to the ferromagnetic configuration within GGA+U/PAW and Heisenberg Model. For GGA+U/PAW, we used optimized structure with $U_{\text{eff}} = 4.72$ eV. For Heisenberg model, we used exchange parameters from optimized structure GGA+U/PAW with $U_{\text{eff}} = 4.72$ eV.

Method	GGA+U/PAW	Heisenberg Model
AFM-I	-0.544	-0.368
AFM-II	-16.264	-16.217
AFM-III	-7.068	-6.954
AFM-IV	-1.071	-1.147
AFM-V	-5.848	-5.991
AFM-VI	-10.440	-10.410
AFM-VII	-5.759	-5.778
AFM-VIII	-5.544	-5.584
AFM-IX	-7.956	-7.974
AFM-X	-2.817	-2.953
AFM-XI	-3.051	-3.087